Smart Structures and Systems, *Vol. 27, No. 3 (2021) 479-492*
DOI: https://doi.org/10.12989/sss.2021.27.3.479

Experimental and numerical investigation of the effect of bridge area and its angularities on the failure mechanism of non-persistent crack in concrete-like materials

Alireza Bagher Shemirani [1], M.S. Amini [2], V. Sarfarazi*[3], K. Shahriar [2], P. Moarefvand [2] and Hadi Haeri [4]

[1] *Faculty of Civil, Water & Environmental Engineering, Shahid Beheshti University, Tehran, Iran*
[2] *Department of Mining and metallurgical engineering, Amirkabir university, Tehran, Iran*
[3] *Department of Mining Engineering, Hamedan University of Technology, Hamedan, Iran*
[4] *State Key Laboratory for Deep GeoMechanics and Underground Engineering, Beijing, 100083, China*

(*Received June 30, 2020, Revised November 10, 2020, Accepted November 22, 2020*)

Abstract. Experimental and discrete element methods were used to investigate the effects of distance between two pre-existing cracks, bridge area (The length of the bridge area) and its angularities on the shear behaviour of bridge area. A punch-through shear test was used to model the gypsum (concrete like) cracks under shear loading. Gypsum samples (concrete like) with dimension of 120 mm × 120 mm × 50 mm were prepared in the laboratory. Within the specimen model and near its four corners, four vertical notches were provided. Three different configuration systems were prepared for notches; i.e., paralell and in plane, inside echelon and outside echelon configuration systems, respectively. In these configurations, the length of cracks were taken as 2 cm, 4 cm and 6 cm based on the cracks configuration systems. Then, 9 specimens with different lengths of the bridge area and bridge area angles were prepared. Assuming a plane strain condition, special rectangular models were prepared with dimensions of 100 mm × 100 mm. similar to those for cracks configuration systems in the experimental tests i.e., 9 models with different lengths of the bridge area and bridge area angularities were prepared. The axial load was applied to the punch through the central portion of the model. This testing showed that the failure process was mostly governed by the lengths of the bridge area and bridge area angularities. The shear strengths of the specimens were related to the fracture pattern and failure mechanism of the discontinuities. It was shown that the shear behaviour of discontinuities is related to the number of the induced tensile cracks which are increased by increasing the lengths of the bridge area. The strength of samples decreases by increasing the crack length. Also, the outside echelon crack configuration system has the maximum value of strength while the inside echelon crack configuration system has the minimum value of specimen's tensile strength. The failure pattern and failure strength are similar in both methods i.e., the experimental testing and the numerical simulation methods.

Keywords: punch-through shear test; lengths of the bridge area; bridge area inclinations; PFC2D

1. Introduction

The compressive and shear behaviours of concretes structures may be governed by the discontinuities and non-persistent cracks existing or induced in these structures under different loading conditions (Eberhardt *et al*. 2002). These non-persistence cracks may have different geometries and bear complicated mechanical treatments affecting the stability and durability of the engineering structures. Many researchers around the world tried to study the mechanical behaviour of discontinuities and cracks in rocks and concetes through experimental tets cariied out in the labolratories (Kim *et al*. 2007, Lin *et al*. 2000, Sarfarazi and Haeri 2016, Sarfarazi *et al*. 2016a, b, 2017, Vasarhelyi and Bobet 2000, Shang *et al*. 2016, Roy *et al*. 2017, Shang *et al*. 2018a, b and c). The cracks initiation, cracks propagation and their coeleasences in the laboratory specimens containining a few open flaws considering various loading conditions have been studied by many researchers (Wong and Einstein 2009a, b, Liu *et al*. 2008, Zhang and Wong 2013, Bahaaddini *et al*. 2013, Abrishambaf *et al*. 2015, Alhussainy *et al*. 2016, Kumar *et al*. 2017, Liu *et al*. 2018, 2018a, b and c, Aliabadian *et al*. 2019). However, in the most of these experimental tests measuring the failure mechanism of bridge area (the intact material in between the concrete like cracks) in the rock and concrete samples under various loading conditions was amongst the most difficult measuring tasks. Therefore, several numerical methods such as finite element methods (e.g., extended finite element method), boundary element methods (e.g., direct methods such as dual boundary element methods and indirect methods such as displacement discontinuity method) and finite difference methods (e.g., discrete element method) were developed to alternatively simulate most of engineering fracture mechanics problems related to laboratory tests and rock engineering problems considering the failure behaviour and fracturing mechanism of non-persistent cracks, discontinuities and cracks problems (Hosseini_Nasab and Fatehi Marji 2007, Zhang *et al*. 2009,

*Corresponding author, Ph.D., Associate Professor,
E-mail: vahab.sarfarazi@gmail.com

ISSN: 1738-1584 (Print), 1738-1991 (Online)

Marji 2013, 2014, 2015, Bi *et al*. 2016, Niu *et al*. 2019, Zhou *et al*. 2015, 2016, Wang *et al*. 2016, Shang *et al*. 2018a, b and c, Zhang *et al*. 2019, Zhou *et al*. 2019, 2020, Shang 2020). The versatile discrete element method (DEM) originally developed by Cundall and Strack (1979) is based on the explicite finite difference approach and proved to be an appropriate simulation technic for modelling the concrete like specimens and investigating the mechanical behaviors of geo-materials used in many rock engineering applications. In a particular version of DEM, known as particle flow code in two dimensions (PFC2D) and three dimensions (PFC3D) the material consisting the concrete like specimens is envisioned as an assembly of elements representing the circular discs (in 2D case) and spherical particles (in 3D case), respectively. The micro-mechanical properties associated with the numerical simulations of modeled specimens with PFC3D need to be calibrated for a contact bonded particle model as explained by Sagong and Bobet (2002). They established a cracked (concrete like) model in their analyses implementing the effect of closed flaws and studied the mechanical behaviour of this cracked (concrete like) model assuming a uniaxial loading condition. They obtained a good relation between the micro and macro mechanical parameters of the modeled (concrete like) specimens. By removing some of the particles at the specified location within an assembly the open flaws can be produced for crack modeling (Ghazvinian *et al*. 2012, Sarfarazi *et al*. 2014). The crack initiation and propagation process can be studied considering one, two and three open flaws in a specified modelled (concrete like) specimen as explained by Zhang and Wong (2013). In this procedure, most of the modelled crack propagation process simulated by the proposed numerical method are similar to those measured experimentally through laboratory tests. Another modeling procedure known as the smooth-crack model can be used to study the mechanical behaviour of the cracked (concrete like) specimens using PFC. Bahaaddini *et al*. (2013) used the smooth-crack model in a bonded particle algorithm to investigate the effect of crack geometry on the mechanism of fraturing process in brittle materilas (concrete like) containing non-persistent cracks. In the present work, the specially designed specimens for a Punch Through Shear (PTS) test are being modelled by the discrete element code to study the mechanical and shear behaviour of non-persistent cracks. The macro mechanical properties of gypsum (concrete like) specimens used for the numerical simulations are being measured through the uniaxial compression and Brazilian tensile tests in the laboratory. The iterative semi-inverse modeling approach adopted in PFC3D is used to calibrate the shear strength and shear behaviour of the bridge area estimated by this numerical modelling technic. The experimental results measured from PTS tests are compared with the corresponding numerical results which verify a very good agreements between these two sets of results.are compared.

2. Stages of laboratory tests

The mechanical properties of the specially prepared lab specimens are obtained in the laboratory by performing some useful simple tests. The gypsum (concrete like) specimens are prepared by the proper mixture of gypsum and water in the mechanics laboratory.

2.1 Mechanical properties of samples

To build the samples, the gypsum and water mixture was used with a ratio of 2 to 1. uniaxial and brazilian tests were carried out on cylindrical samples and disc samples. The cylindrical samples have a diameter of 54 mm and the height of 108 mm. The disc samples have a diameter 54 and the thickness of 27 mm. The loading rate was 0.01 mm/sec. Figs. 1(a) and (b) shows failure pattern in uniaxial test and Brazilian test. Fig. 1(c) shows the stress-strain curve of gypsum (concrete like) specimens. Table 1 shows compressive strength and tensile strength of concrete like specimens.

2.2 How to build specimens containing non-persistent cracks

The specimens containing non-persistence cracks were prepared in the laboratory, by mixing gypsum and water with a ratio of 2-1, respectively. Special molds were provided

Table 1 Mechanical properties of specimens

Compressive strength	7.2 MPa
Tensile strength	1.3 MPa

(a) (b) (c)

Fig. 1 (a) failure pattern in experimental test; (b) failure pattern in Brazilian test; (c) the stress-strain curve of gypsum (concrete like) specimens

(a)

(b)

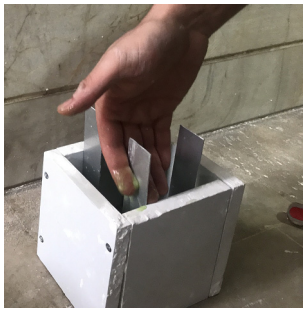

(c)

(d)

(e)

(f)

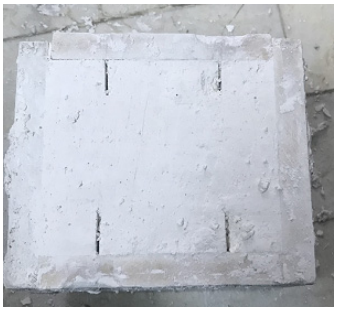

(g)

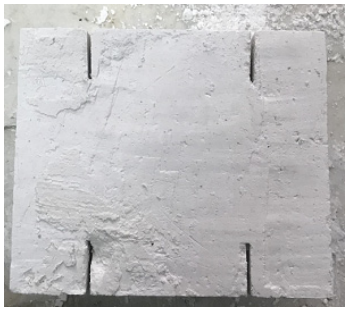

(h)

Fig. 2 (a) A special black plastic fiber with dimension of 10 cm × 10 cm × 5 cm was put into the frame; (b) the shime inside the plastic fiber; (c) Grace around the shime; (d) adjustment the shime inside the frame; (e) plaster slurry inside the mold; (f) the aluminum sheet is removed from the mold; (g) the specimen consisting non-persistent crack inside the frame; (h) the specimen consisting non-persistent crack outside the frame

and the mixture of gypsum and water was poured into them for being casted at a specified time period. The specimen casting procedure has a special framework with the dimensions of 10 cm × 10 cm × 15 cm (Fig. 2(a)). This framework was made from fiberglass in order to be waterproof and also do not observe the water to decrease the effective volume of the mold for producing the standard casted specimens. A special plastic fiber of dimensions 10 cm × 10 cm × 5 cm was placed into the frame as shown in Fig. 2(b). Then, as shown in Fig. 2(c), the aluminum sheets were moved to Grace which was inserted from one side into the plastic fiber and from other side it was connected to the free surface (Fig. 2(d)). The attachment of the blade to the chalk is hold by the Grace. After about 15 minutes, the plaster can be removed from the mold (Fig. 2(e)) i.e., the aluminum sheet was removed from the mold

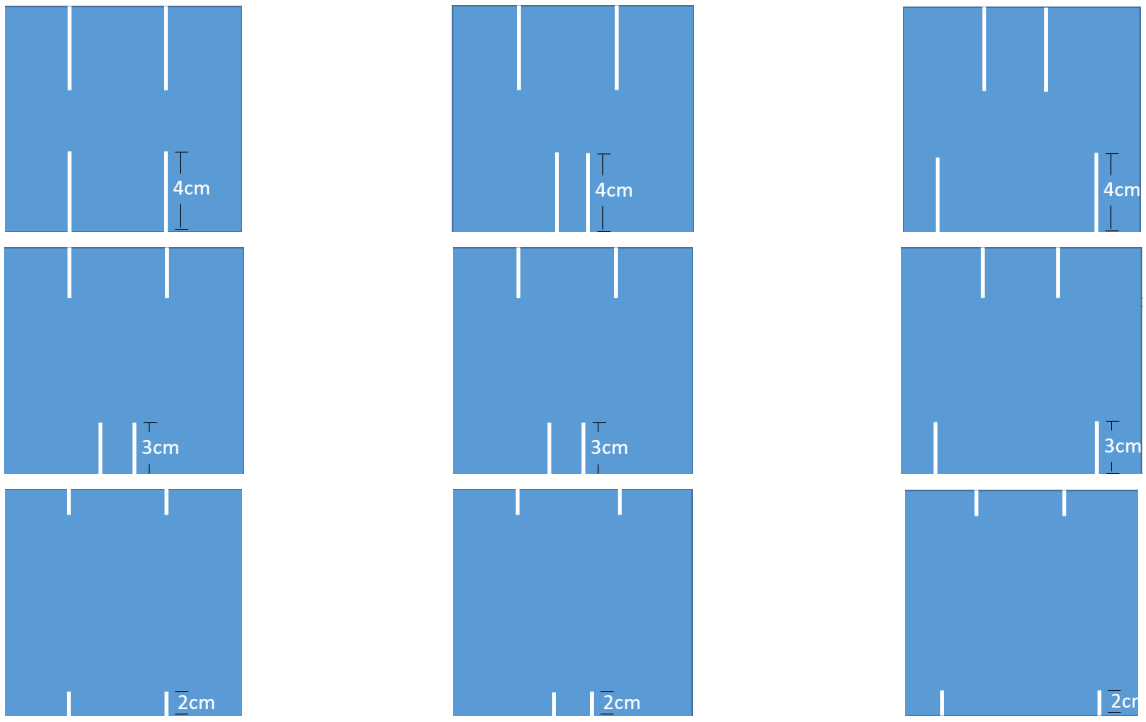

(a) (b) (c)

Fig. 3 (a) Bridge area angle is 0° (in plate parallel crack); (b) bridge area angle is 30° (inside echelon crack); (c) bridge area angle is 60° (outside echelon crack)

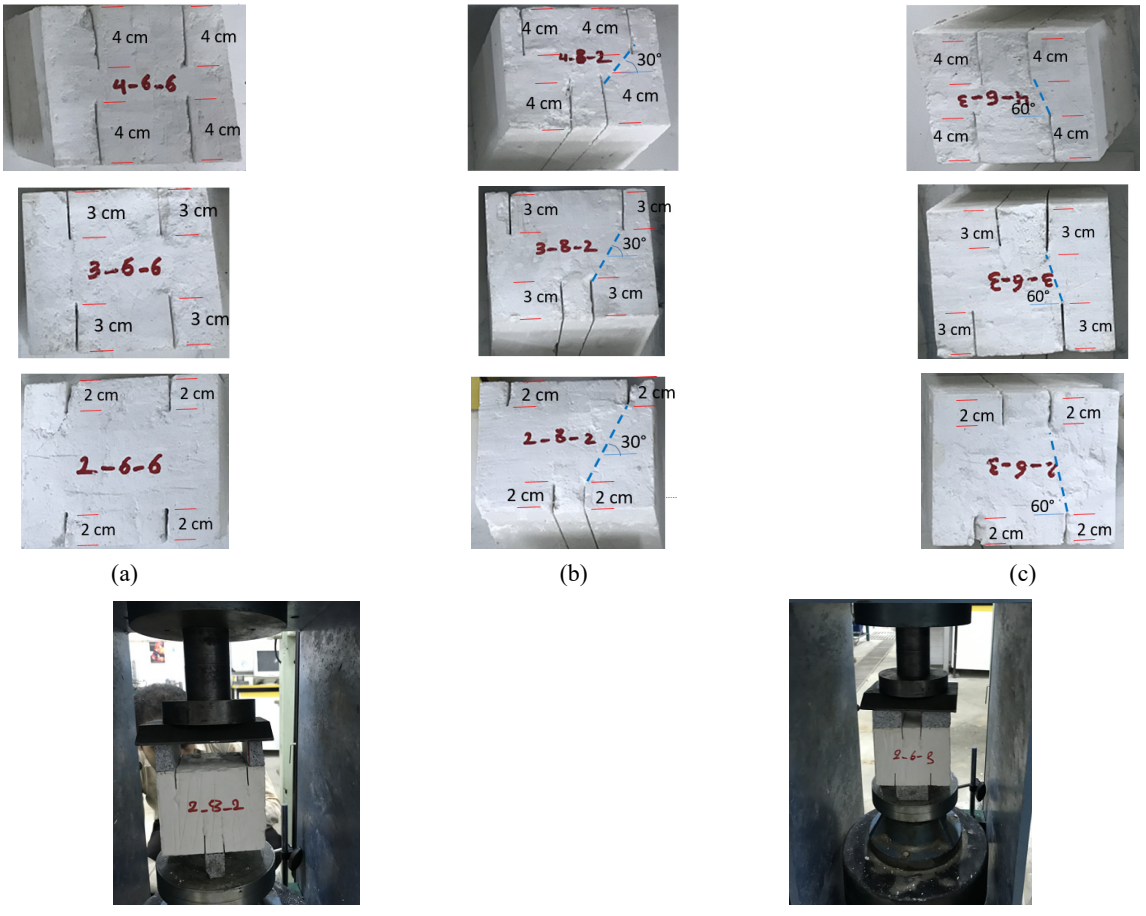

(a) (b) (c)

(d) (e)

Fig. 4 (a) Bridge area angle is 0° (in plate parallel crack); (b) bridge area angle is 30° (inside echelon crack); (c) bridge area angle is 60° (outside echelon crack); (d) Inside echelon configuration; (e) out-side echelon configuration

(Fig. 2(f)), the cast bolts were then opened (Fig. 2(g)) and the prepared samples were removed from the mold (Fig. 2(h)). The casted samples should be kept in the laboratory for about 15 days at the room temperature. Then these specimens can be used for uniaxial compression or any other laboratory tests to measure their required mechanical properties. Several types of specimens can be made in the laboratory. In general, the specimens containing two non-persistent cracks were constructed in this study (Fig. 3). Several bridge area angularities with three different angles, i.e., 0° (Fig. 4(a)), 30° (Fig. 4(b)) and 60° (Fig. 4(c)) were studied. Then, for each bridge area configuration, three crack lengths i.e., 2 cm, 3 cm and 4 cm were selected as shown in Fig. 4. Therefore, based on these bridge area angularities, three different cracks configurations have been defined i.e., in plane parallel crack system (Fig. 4(a)); inside echelon crack system (Fig. 4(b)) and outside echelon crack system (Fig. 4(c)).

2.3 Loading the specimen

In order to carry out loading on the specimens, the specimens are placed inside the uniaxial machine. Then granite specimens are placed between the specimen and the plates of the loading machine (Fig. 4). The loading rate is 0.005 mm/s.

3. Experimentally observed failure patterns

In this study, some experimental work was carried out to observe the failure pattern of the specimens containing non-persistence cracks with different bridge areas configurations.

3.1 Failure mechanism of samples

Fig. 5 shows the failure pattern of specimens containing non - persistent crack with bridge area angularity of 0°. When crack lengths were 2 cm (Fig. 5(a)), one tensile crack initiated from lower tip of the crack and propagated parallel to loading axis till coalescence with upper boundary of samples. When crack lengths were 3 cm (Fig. 5(b)), two tensile crack initiated from the crack tips and propagated parallel to loading axis till coalescence with other crack tips. When crack lengths were 4 cm (Fig. 5(c)), two tensile crack initiated from the crack tips and propagated parallel to loading axis till coalescence with other crack tips.

Fig. 6 shows the failure pattern of specimens containing non - persistent crack with bridge area angularity of 30° (inside echelon cracks). When crack lengths were 2 cm (Fig. 6(a)), one tensile crack initiated from tip of the lower crack and propagated parallel to loading axis till coalescence with upper boundary of samples. When crack lengths were 3 cm (Fig. 6(b)), two tensile crack initiated from the crack tips and propagated parallel to loading axis till coalescence with other crack tips. When crack lengths were 4 cm (Fig. 6(c)), two tensile crack initiated from the crack tips and propagated parallel to loading axis till coalescence with other crack tips.

Fig. 7 shows the failure pattern of specimens containing non-persistent crack with bridge area angularity of 60° (out side echelon cracks). When crack lengths were 2 cm (Fig. 7(a)), one tensile crack initiated from tip of the upper crack and propagated parallel to loading axis till coalescence with upper boundary of samples. When crack lengths were 3 cm (Fig. 7(b)), one tensile crack initiated from the crack tips and propagated parallel to loading axis till coalescence with

(a) (b) (c)

Fig. 5 Shows the failure pattern of specimens with crack lengths of; (a) 2 cm; (b) 3 cm; and (c) 4 cm

(a) (b) (c)

Fig. 6 Shows the failure pattern of specimens with inside echelon crack configuration. crack lengths is: (a) 2 cm; (b) 3 cm; and (c) 4 cm

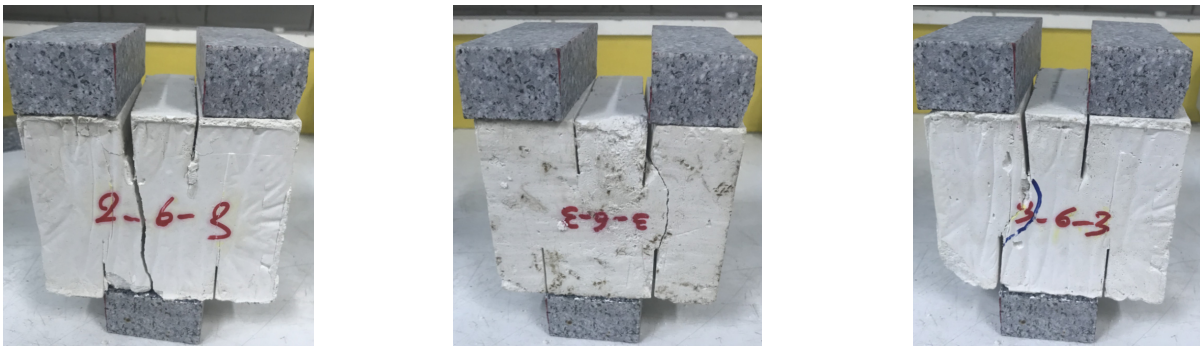

(a) (b) (c)

Fig. 7 Shows the failure pattern of specimens with outside echelon crack configuration. crack lengths is: (a) 2 cm; (b) 3 cm; and (c) 4 cm

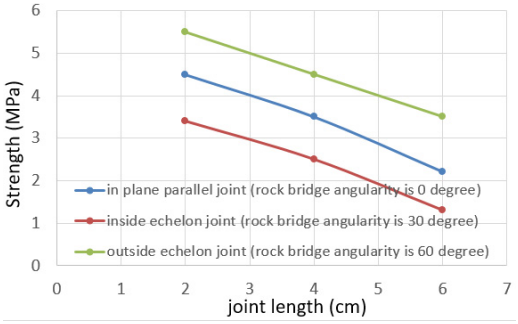

Fig. 8 The effect of crack length on the strength of samples for different crack configuration; i.e., in plane parallel crack, inside echelon crack and outside echelon crack

other crack tips. When crack lengths were 4 cm (Fig. 7(c)), one tensile crack initiated from the crack tips and propagated parallel to loading axis till coalescence with other crack tips.

3.2 The effect of crack length on the strength of samples

Fig. 8 shows the effect of crack length on the strength of samples for different crack configuration; i.e., in plane parallel crack, inside echelon crack and outside echelon crack.

The strength of samples decreases by increasing the crack length. Also, the outside echelon crack has maximum value of strength while inside echelon crack configuration has minimum value of tensile strength. In fact, bridge area is under compressive force in outside echelon crack configuration while it is under tensile force in inside echelon crack configuration.

4. The discrete element modelling of concrete like specimens

The discrete element method used in form of a two dimensional particle flow code (PFC2D) for the simulation of cracked concrete like specimens in this research. In this modeling approach, the concrete like material is considered as an assembly of rigid particles which are in contact with each other at a specified points and can move independently within the assembly (Potyondy and Cundall 2004). A central finite difference algorithm applied in the discrete element approach and adopted in the particle flow code to calculate the interaction forces and relative movements of the particles within the assembly. When tensile force or shear force exceed to tensile strength and shear strength of discs bonds, the bond breaks and one crack initiate at this place (Fig. 9). The limitations of DEM as mentioned by Donze *et al*. (2009) are: (a) Fracture is closely related to the size of elements, and that is so called size effect. (b) Cross effect exists because of the difference between the size and shape of elements with real grains. (c) In order to establish the relationship between the local and macroscopic constitutive laws, data obtained from classical geomechanical tests which may be impractical are used.

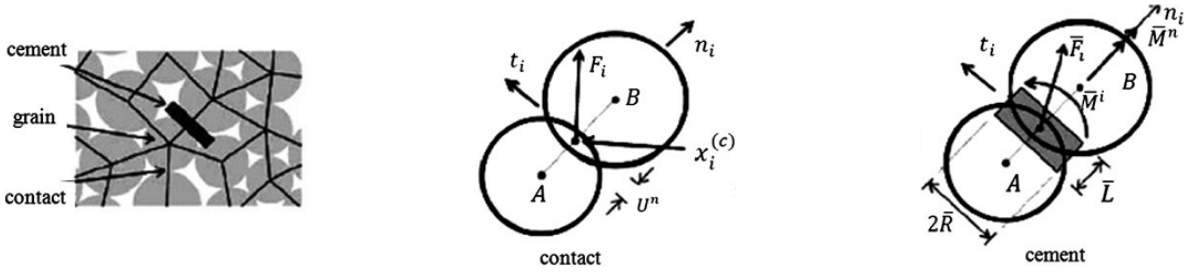

(a) (b) (c)

Fig. 9 The force-displacement relationship for the bonding particle system (Potyondy and Cundall 2004)

4.1 Preparation and Calibration of the PFC2D Model for Concrete-Like Material:

The standard process of generating a PFC2D assembly to represent a test model, used in this article, is described in detail by Potyondy and Cundall (2004). The process involves: particle generation, packing the particles, isotropic stress installation (stress initialization), floating particle (floater) elimination and bond installation. A gravity effect did not need to be considered as the specimens were small, and the gravity-induced stress gradient had a negligible effect on the macroscopic behavior. Uniaxial compressive strength and Brazilian test were carried out to calibrate the properties of particles and parallel bonds in bonded particle model (Ghazvinian *et al*. 2012). Adopting the micro-properties listed in Table 2 and the standard calibration procedures (Potyondy and Cundall 2004), a calibrated PFC particle assembly was created. Fig. 10(a) and (b) shows the experimental uniaxial compression test and numerical simulation, respectively. Also, Figs. 10(c) and (d) shows experimental Brazilian test and numerical simulation, respectively. The results show well matching between experimental test and numerical simulation.

4.2 Numerical compressive tests on the non-persistent open crack

After calibration of PFC2D, punch shear tests for cracked concrete like were numerically simulated by creating a box model in the PFC2D (by using the calibrated micro-parameters) (Fig. 11). The PFC specimen had the dimensions of 100 mm × 100 mm. A total of 13168 disks with a minimum radius of 0.27 mm were used to make up the box specimen. Two walls exist at the upper and lower of the model. The non-persistent cracks were formed by deletion of bands of particles from the model. The opening

Table 2 Micro properties used to represent the intact concrete like

Parameter	Value	Parameter	Value
Type of particle	Disc	Parallel-bond radius multiplier	1
Density (kg/m^3)	3000	Young's modulus of parallel bond (GPa)	4
Minimum radius (mm)	0.27	Parallel bond stiffness ratio	1.7
Size ratio	1.56	Particle friction coefficient	0.4
Porosity ratio	0.08	Parallel bond normal strength, mean (MPa)	7.6
Damping coefficient	0.7	Parallel bond normal strength, SD (MPa)	1.4
Contact Young's modulus (GPa)	4	Parallel bond shear strength, mean (MPa)	7.6
Stiffness ratio	1.7	Parallel bond shear strength, SD (MPa)	1.4

(a)

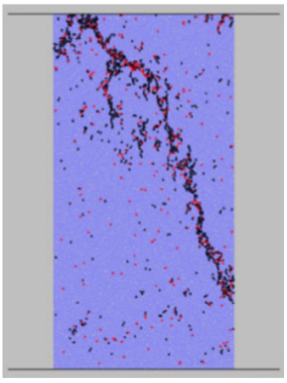

(b)

(c)

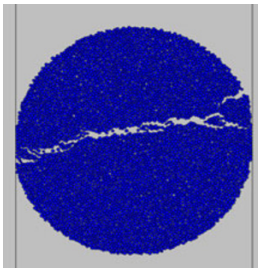

(d)

Fig. 10 (a) Experimental compression test; (b) numerical compression test; (c) experimental Brazilian test; and (d) numerical Brazilian test

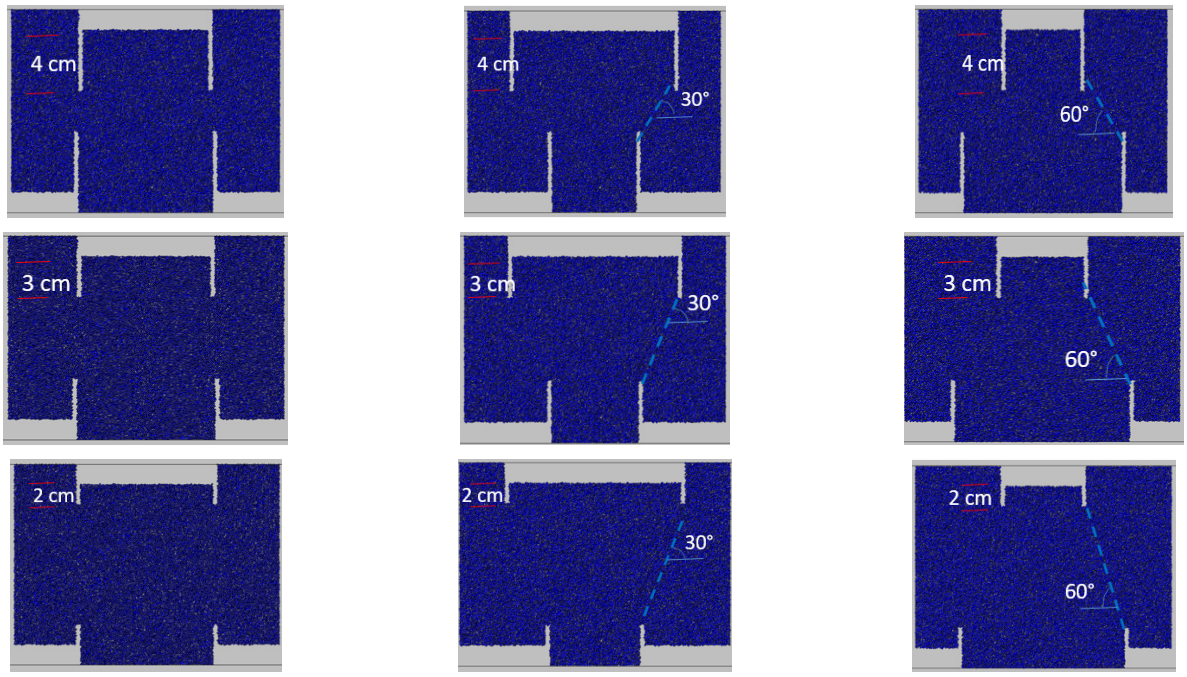

(a) (b) (c)

Fig. 11 (a) Bridge area angle is 0° (in plate parallel crack); (b) bridge area angle is 30° (inside echelon crack); (c) bridge area angle is 60° (outside echelon crack)

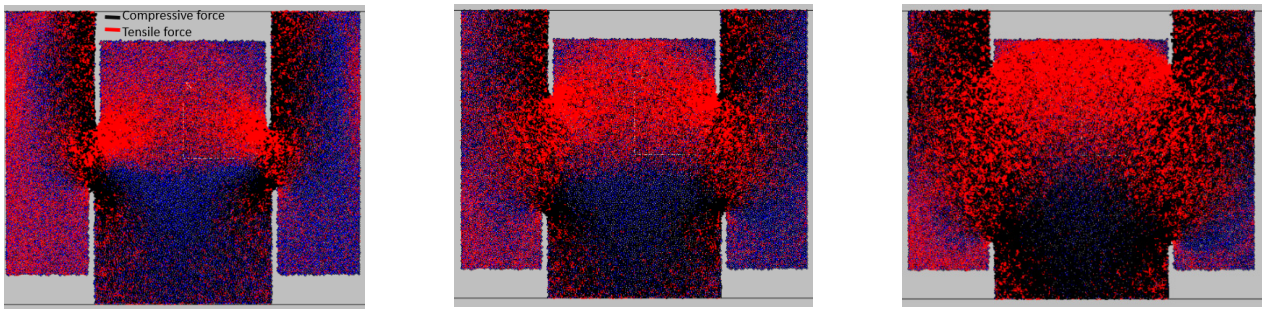

(a) (b) (c)

Fig. 12 The parallel bond force distribution in in-plane parallel crack configuration; crack length was (a) 4 cm; (b) 3 cm; and (c) 2 cm

of these notches is 1 mm (Fig. 11). In general, the models containing two non – persistent cracks were constructed. The bridge area angularities changed in three different values; i.e., 0° (Fig. 11(a)), 30° (Fig. 11(b)) and 60° (Fig. 11(c)). For each bridge area configuration, crack lengths were 2 cm, 3 cm and 4 cm (Fig. 11). Based on the bridge area angularities three different configuration have been defined; i.e., in plate parallel crack (Fig. 11(a)), inside echelon crack (Fig. 11(b)) and outside echelon crack (Fig. 11(c)). It should be noticed that this crack configuration is similar to experimental one. Upper and lower walls applied uniaxial force on the model. The compression force was registered by taking the reaction forces on the upper wall.

4.3 The modelled parallel bond forces before the crack initiation process

The parallel bond force distribution (as shown in Figs. 12-14) illustrates the state of force vectors within the modelled samples before the crack initiation process for three configuration of non-persistent crack; i.e., in plane parallel crack (Fig. 12), outside echelon crack (Fig. 13) and inside echelon crack (Fig. 14). The red and dark lines shown in Figs. 12-14 represent the tensile and compression force vectors in the model, respectively. The coarse lines and their accumulation show the areas where larger forces are induced within the model. It can be easily seen that the tensile forces of the bonded particles at the tip of the crack are less than their shear strength, therefore, the tensile crack initiation is a dominant mode of fracturing that initiates at the tip of the crack within the modelled samples. It's to be noticed that the compressive force was distributed in the bridge area in out-side crack configuration while the tensile force was distributed in the bridge area in in-side crack configuration.

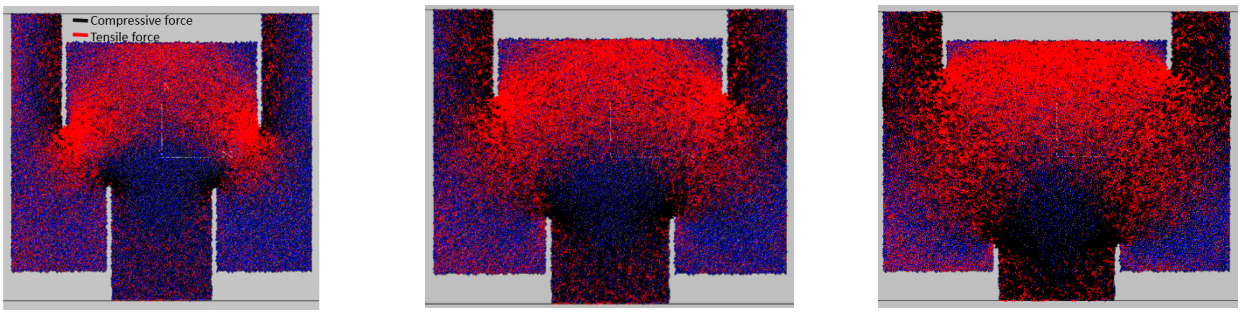

(a) (b) (c)

Fig. 13 The parallel bond force distribution in inside echelon crack configuration; crack length was (a) 4 cm; (b) 3 cm; and (c) 2 cm

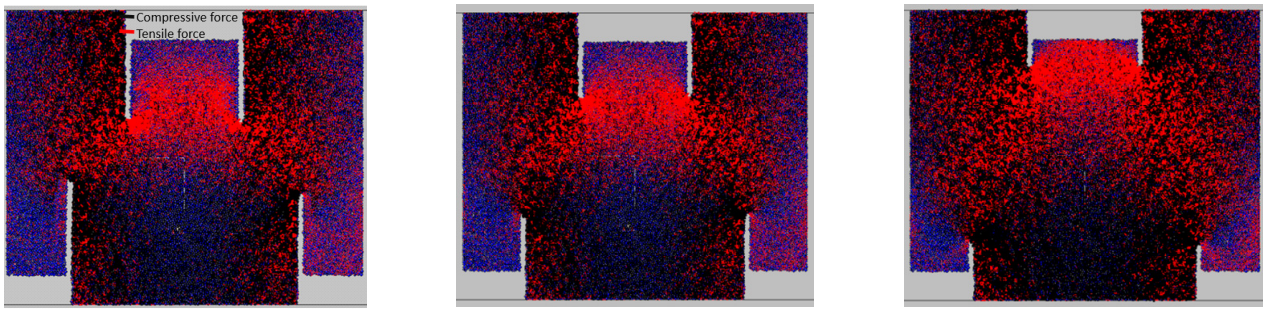

(a) (b) (c)

Fig. 14 The parallel bond force distribution in outside echelon crack configuration; crack length was (a) 4 cm; (b) 3 cm; and (c) 2 cm

4.4 The distribution of displacement vectors in the modeled samples

The distribution of particle displacement vectors in the modelled sample is shown in Fig. 15-17. The typical displacement vector observed in the Brazilian tensile test simulation using the same micro-parameters as in the punch through shear test is shown in Fig. 18. The displacement vectors of the particles in a modelled sample illustrate how the particles are moving as they are subjected to the external loading conditions. Figs. 15-18 illustrates that in both the punch through shear test and the Brazilian test, the displacement vectors show similar trends, and the fractures display a tensile mode of failure, characteristic of Mode I fractures (the fracture mechanics terminology for fractures subjected to tensile loading conditions).

4.5 The effects of crack configuration on the failure behavior of the modelled samples

The fracture patterns of the modelled samples with the different crack configuration are considered to study the effects of bridge area angularities and join length on fracturing process of the brittle materials in a punch through shear test.

a) Failure mechanism of the model with in-plane parallel crack configuration (bridge area angularity was 0°)

In the failure mechanism of the modelled samples with

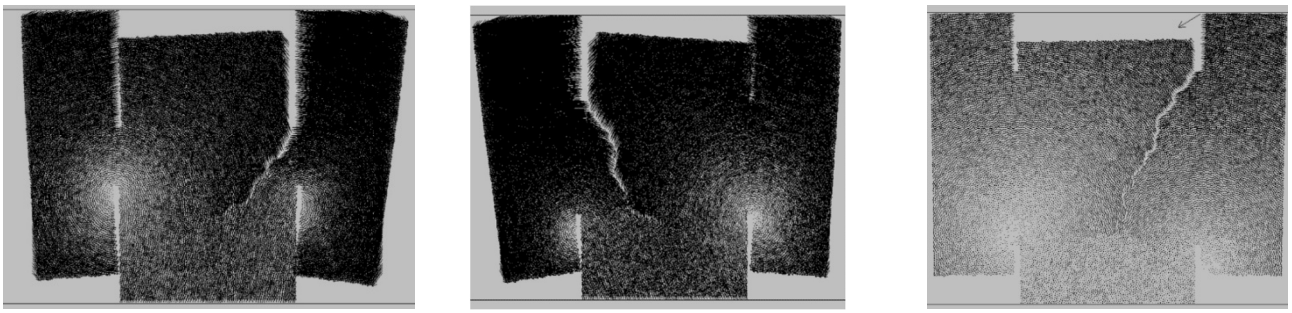

(a) (b) (c)

Fig. 15 The particle displacement vectors in in-plane parallel crack configuration; crack length was (a) 4 cm; (b) 3 cm; and (c) 2 cm

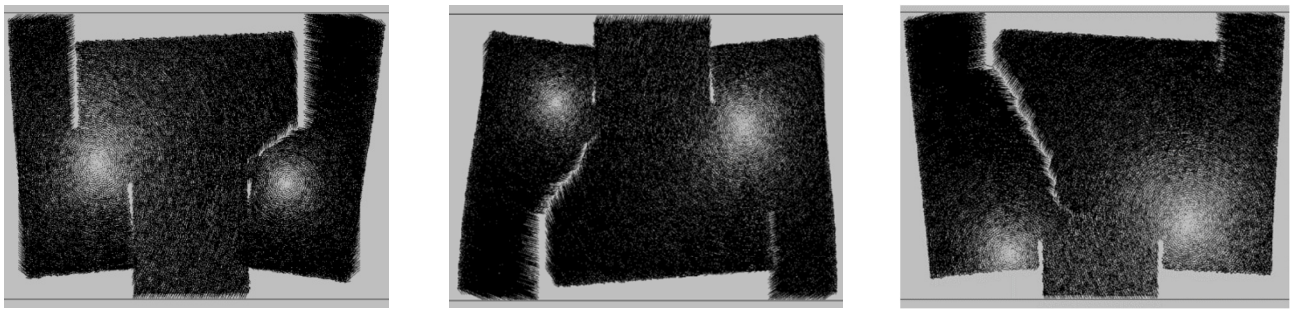

(a) (b) (c)

Fig. 16 The particle displacement vectors in inside echelon crack configuration; crack length was (a) 4 cm; (b) 3 cm; and (c) 2 cm

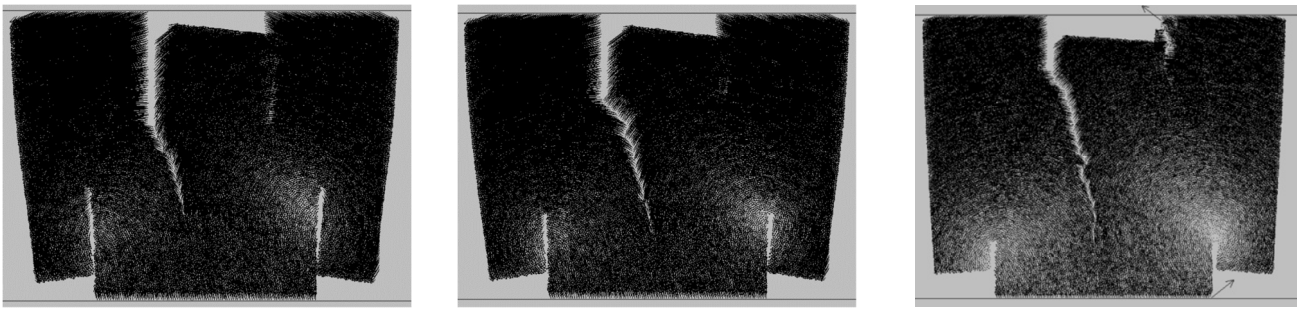

(a) (b) (c)

Fig. 17 The particle displacement vectors in outside echelon crack configuration; crack length was (a) 4 cm; (b) 3 cm; and (c) 2 cm

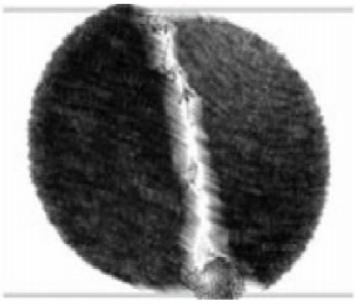

Fig. 18 The displacement vectors observed in a Brazilian tensile test

different in-plane parallel crack length (Fig. 19(a)-(c)), the tensile wing cracks may initiate from the crack tip and propagate diagonally with respect to the direction of shear loading. Due to the lower tensile strength of the modelled samples the tensile cracks are the most dominant mode of failure compared to those of shear mode. At the peak shear loading condition, the branching occurs in wing crack.

b) Failure mechanism of the model with inside echelon crack configuration (bridge area angularity was 30°)

In the failure mechanism of the modelled samples with different inside echelon crack length (Figs. 20(a)-(c)), the

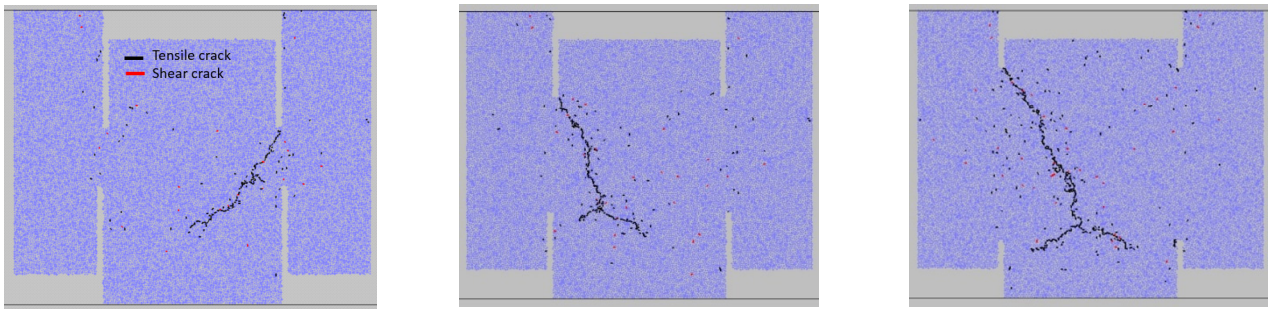

(a) (b) (c)

Fig. 19 The particle displacement vectors in in-plane parallel crack configuration; crack length was (a) 4 cm; (b) 3 cm; and (c) 2 cm

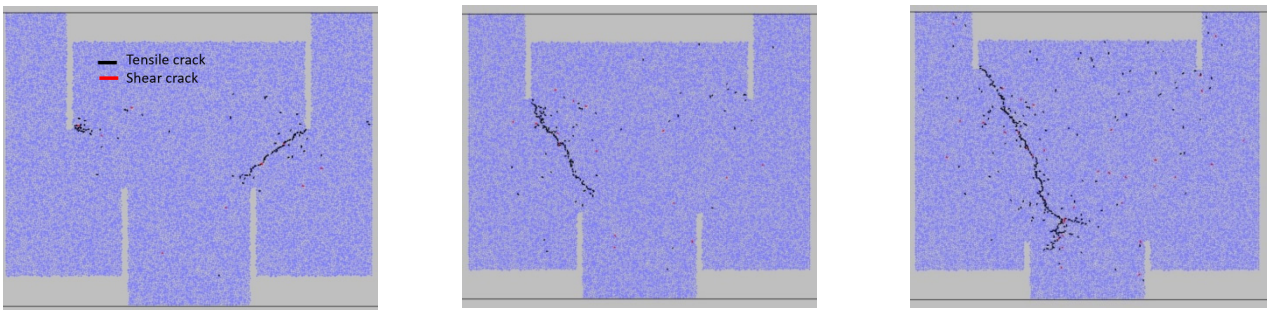

(a) (b) (c)

Fig. 20 The particle displacement vectors in inside echelon crack configuration; crack length was (a) 4 cm; (b) 3 cm; and (c) 2 cm

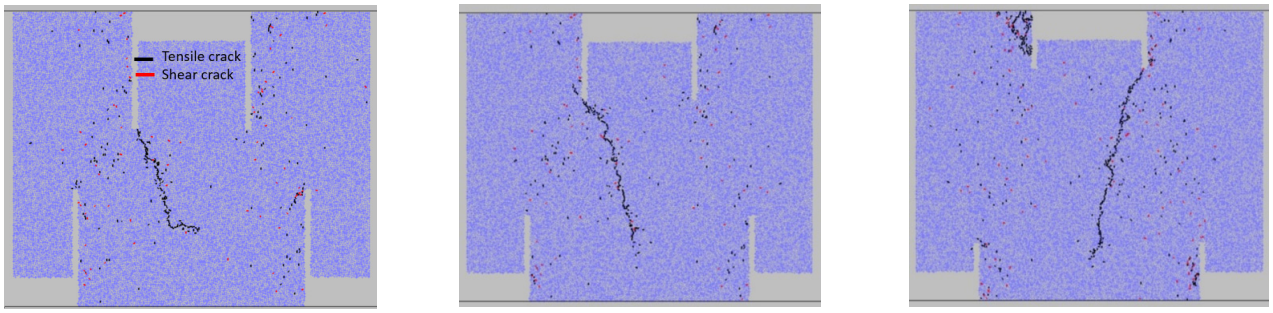

(a) (b) (c)

Fig. 21 The particle displacement vectors in outside echelon crack configuration; crack length was (a) 4 cm; (b) 3 cm; and (c) 2 cm

tensile wing cracks may initiate from the crack tip and propagate diagonally with respect to the direction of shear loading till coalescence with another join tip. Due to the lower tensile strength of the modelled samples the tensile cracks are the most dominant mode of failure compared to those of shear mode.

c) Failure mechanism of the out-side echelon crack configuration model (bridge area angularity was 60°)

In the failure mechanism of the modelled samples with different out-side echelon crack length (Figs. 21(a)-(c)), the tensile wing cracks may initiate from the crack tip and propagate diagonally with respect to the direction of shear loading. Due to the lower tensile strength of the modelled samples the tensile cracks are the most dominant mode of failure compared to those of shear mode.

By comparison between Figs. 5-7 and Figs. 19-21, I can be concluded that failure pattern is similar in both of the experimental test and numerical simulation.

4.6 The effect of crack length on the strength of samples

Fig. 22 shows the effect of crack length on the strength of models with three different crack configuration; i.e., in plane parallel crack, inside echelon crack and outside echelon crack.

The strength of samples decreases by increasing the crack length. Also, the outside echelon crack has maximum

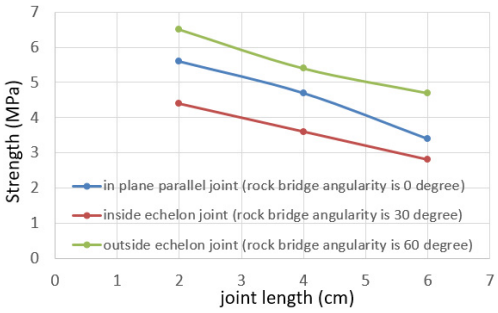

Fig. 22 The effect of crack length on the strength of models for different crack configuration; i.e., in plane parallel crack, inside echelon crack and outside echelon crack

value of strength while inside echelon crack configuration has minimum value of tensile strength. In fact, bridge area is under compressive force in outside echelon crack configuration (Fig. 14) while it is under tensile force in inside echelon crack configuration (Fig. 13).

By comparison between Figs. 8 and 22. It can be concluded that failure strength is nearly similar in both of the experimental test and numerical simulation.

5. Conclusions

- The failure pattern of specimens containing non - persistent crack with bridge area angularity of 0°.

When crack lengths were 2 cm, one tensile crack initiated from lower tip of the crack and propagated parallel to loading axis till coalescence with upper boundary of samples. When crack lengths were 3 cm, two tensile cracks initiated from the crack tips and propagated parallel to loading axis till coalescence with other crack tips. When crack lengths were 4 cm, two tensile crack initiated from the crack tips and propagated parallel to loading axis till coalescence with other crack tips.

- the failure pattern of specimens containing non - persistent crack with bridge area angularity of 30° (inside echelon cracks). When crack lengths were 2 cm, one tensile crack initiated from tip of the lower crack and propagated parallel to loading axis till coalescence with upper boundary of samples. When crack lengths were 3 cm, two tensile crack initiated from the crack tips and propagated parallel to loading axis till coalescence with other crack tips. When crack lengths were 4 cm, two tensile crack initiated from the crack tips and propagated parallel to loading axis till coalescence with other crack tips.
- The failure pattern of specimens containing non - persistent crack with bridge area angularity of 60° (outside echelon cracks). When crack lengths were 2 cm, one tensile crack initiated from tip of the upper crack and propagated parallel to loading axis till coalescence with upper boundary of samples. When crack lengths were 3 cm, one tensile crack initiated from the crack tips and propagated parallel to loading axis till coalescence with other crack tips. When crack lengths were 4 cm, one tensile crack initiated from the crack tips and propagated parallel to loading axis till coalescence with other crack tips.
- The strength of samples decreases by increasing the crack length. Also, the outside echelon crack has maximum value of strength while inside echelon crack configuration has minimum value of tensile strength.
- The compressive force was distributed in the bridge area in out-side crack configuration while the tensile force was distributed in the bridge area in in-side crack configuration.
- in both the direct shear test and the Brazilian test, the displacement vectors show similar trends, and the fractures display a tensile mode of failure, characteristic of Mode I fractures (the fracture mechanics terminology for fractures subjected to tensile loading conditions).
- Failure pattern is similar in both of the experimental test and numerical simulation.
- Failure strength is similar in both of the experimental test and numerical simulation.
- It's to be note that, Gypsum (concrete like) samples were used in this study. This kind of materials is not representative of natural rocks and concrete because they are aggregates with irregular minerals or particles.

References

Abrishambaf, A., Barros, J.A. and Cunha, V.M. (2015), "Tensile stress–crack width law for steel fibre reinforced self-compacting concrete obtained from indirect (splitting) tensile tests", *Cement Concrete Compos*., **57**, 153-165. https://doi.org/10.1016/j.cemconcomp.2014.12.010

Alhussainy, F., Hasan, H.A., Rogic, S., Sheikh, M.N. and Hadi, M.N. (2016), "Direct tensile testing of self-compacting concrete", *Constr. Build. Mater*., **112**, 903-906. https://doi.org/10.1016/j.conbuildmat.2016.02.215

Aliabadian, Z., Zhao, G.F. and Russell, A.R. (2019), "Failure, crack initiation and the tensile strength of transversely isotropic rock using the Brazilian test", *Int. J. Rock Mech. Mining Sci*., **122**, 104073. https://doi.org/10.1016/j.ijrmms.2019.104073

Bahaaddini, M., Sharrock, G. and Hebblewhite, B.K. (2013), "Numerical investigation of the effect of crack geometrical parameters on the mechanical properties of a non-persistent cracked rock mass under uniaxial compression", *Comput. Geotech*., **49**, 206-225. https://doi.org/10.1016/j.compgeo.2012.10.012

Bi, J., Zhou, X.P. and Qian, Q.H. (2016), "The 3D numerical simulation for the propagation process of multiple pre-existing flaws in rock-like materials subjected to biaxial compressive loads", *Rock Mech. Rock Eng*., **49**, 1611-1627. https://doi.org/10.1007/s00603-015-0867-y

Cundall, P.A. and Strack, O.D.L. (1979), "A discrete numerical model for granular assemblies", *Geotechnique*, **29**(1), 47-65. https://doi.org/10.1680/geot.1979.29.1.47

Donzé, F.V., Richefeu, V. and Magnier, S.A. (2009), "Advances in discrete element method applied to soil rock and concrete mechanics", *Electron. J. Geol. Eng*., **8**, 1-44.

Eberhardt, E., Stead, D., Coggan, J. and Willenberg, H. (2002), "An integrated nu-merical analysis approach to the Randa rockslide", *Proceedings of the First European Conference on Landslides*, Prague, Czech Republic, June, pp. 355-332.

Ghazvinian, A., Sarfarazi, V., Schubert, W. and Blumel, M. (2012), "A study of the failure mechanism of planar non-persistent open cracks using PFC2D", *Rock Mech. Rock Eng*., **45**(5), 677-693. https://doi.org/10.1007/s00603-012-0233-2

Hosseini_Nasab, H. and Fatehi Marji, M. (2007), "A semi-infinite higher-order displacement discontinuity method and its application to the quasistatic analysis of radial cracks produced by blasting", *J. Mech. Mater. Struct*., **2**(3), 439-458. https://doi.org/10.2140/jomms.2007.2.439

Kim, B.H., Kaiser, P.K. and Grasselli, G. (2007), "Influence of persistence on behavior of fractured rock masses", *Geological Society*, *London*, *Special Publications*, **284**(1), 161-173. https://doi.org/10.1144/SP284.11

Kumar, M., Rana, S., Pant, P.D. and Patel, R.C. (2017), "Slope stability analysis of Balia Nala landslide, Kumaun lesser Himalaya, Nainital, Uttarakhand, India", *Journal of Rock Mechanics and Geotechnical Engineering*, **9**(1), 150-158. https://doi.org/10.1016/j.jrmge.2016.05.009

Li, S., Wang, H., Li, Y., Li, Q., Zhang, B. and Zhu, H. (2016), "A new mini-grating absolute displacement measuring system for static and dynamic geomechanical model tests", *Measurement*, **105**, 25-33. https://doi.org/10.1016/j.measurement.2017.04.002

Lin, P., Wong, R.H., Chau, K.T. and Tang, C.A. (2000), "Multi-crack coalesence in rock-like material under uniaxial and biaxial loading", *Key Eng. Mater*., **183**, 809-814. https://doi.org/10.4028/www.scientific.net/KEM.183-187.809

Liu, G., Zhao, J., Song, H.W. and Li, Y.H. (2008), "Model experiments on the broken zone in intermittently jointed surrounding rock", *J. China Univ. Mining Technol*., **37**(1), 62-66.

Liu, Y.I., Dai, F., Xu, N., Zhao, T. and Feng, P. (2018), "Experimental and numerical investigation on the tensile fatigue

properties of rocks using the cyclic flattened Brazilian disc method", Soil Dynamics and Earthquake Engineering, **105**, 68-82. https://doi.org/10.1016/j.soildyn.2017.11.025

Marji, M.F. (2013), "On the use of power series solution method in the crack analysis of brittle materials by indirect boundary element method", *Eng. Fract. Mech.*, **98**, 365-382.

Marji, M.F. (2014), "Numerical analysis of quasi-static crack branching in brittle solids by a modified displacement discontinuity method", *Int. J. Solids Struct.*, **51**(9), 1716-1736. https://doi.org/10.1016/j.ijsolstr.2014.01.022

Marji, M.F. (2015), "Simulation of crack coalescence mechanism underneath single and double disc cutters by higher order displacement discontinuity method", *J. Central South Univ.*, **22**(3), 1045-1054. https://doi.org/10.1007/s11771-015-2615-6

Niu, Y., Zhou, X.P., Zhang, J.Z. and Qian, Q.H. (2019), "Experimental study on crack coalescence behavior of double unparallel fissure contained sandstone specimens subjected to freeze-thaw cycles under uniaxial compression", *Cold Regions Sci. Technol.*, **158**, 166-181. https://doi.org/10.1016/j.coldregions.2018.11.015

Omar, H., Ahmad, J., Nahazanan, H., Mohammed, T.A. and Yusoff, Z.M. (2018), "Measurement and simulation of diametrical and axial indirect tensile tests for weak rocks", *Measurement*, **127**, 299-307. https://doi.org/10.1016/j.measurement.2018.05.067

Potyondy, D.O. and Cundall, P.A. (2004), "A bonded-particle model for rock", *Int. J. Rock Mech. Mining Sci.*, **41**(8), 1329-1364. https://doi.org/10.1016/j.ijrmms.2004.09.011

Roy, D.G., Singh, T.N. and Kodikara, J. (2017), "Influence of crack anisotropy on the fracturing behavior of a sedimentary rock", *Eng. Geol.*, **228**(13), 224-237. https://doi.org/10.1016/j.enggeo.2017.08.016

Sagong, M. and Bobet, A. (2002), "Coalescence of multiple flaws in a rock-model material in uniaxial compression", *Int. J. Rock Mech. Min. Sci.*, **39**(2), 229-241. https://doi.org/10.1016/S1365-1609(02)00027-8

Sarfarazi, V. and Haeri, H. (2016), "Effect of number and configuration of bridges on shear properties of sliding surface", *J. Min. Sci.*, **52**(2), 245-257. https://doi.org/10.1134/S1062739116020370

Sarfarazi, V., Ghazvinian, A., Schubert, W., Blumel, M. and Nejati, H.R. (2014), "Numerical simulation of the process of fracture of Echelon rock cracks", *Rock Mech. Rock Eng.*, **47**(4), 1355-1371. https://doi.org/10.1007/s00603-013-0450-3

Sarfarazi, V., Faridi, H.R., Haeri, H. and Schubert, W. (2016a), "A new approach for measurement of anisotropic tensile strength of concrete", *Adv. Concrete Constr., Int. J.*, **3**(4), 269-284. https://doi.org/10.12989/acc.2015.3.4.269

Sarfarazi, V., Haeri, H. and Khaloo, A. (2016b), "The effect of non-persistent cracks on sliding direction of rock slopes", *Comput. Concrete, Int. J.*, **17**(6), 723-737. https://doi.org/10.12989/cac.2016.17.6.723

Sarfarazi, V., Haeri, H., Shemirani, A.B. and Zhu, Z. (2017), "Shear behavior of non-persistent joint under high normal load", *Strength Mater.*, **49**, 320-334. https://doi.org/10.1007/s11223-017-9872-6

Shang, J. (2020), "Rupture of veined granite in polyaxial compression: insights from three-dimensional discrete element method modeling", *JGR Solid Earth*, **125**, 1-25. https://doi.org/10.1029/2019JB019052

Shang, J., Hencher, S.R. and West, L.J. (2016), "Tensile strength of geological discontinuities including incipient bedding, rock cracks and mineral veins", *Rock Mech. Rock Eng.*, **49**, 4213-4225. https://doi.org/10.1007/s00603-016-1041-x

Shang, J.L., Zhao, Z.Y. and Ma, S.Q. (2018a), "On the shear failure of incipient rock discontinuities under CNL and CNS boundary conditions: insights from DEM modelling", *Eng. Geol.*, **234**, 153-166. https://doi.org/10.1016/j.enggeo.2018.01.012

Shang, J., Zhao, Z., Hu, J. and Handley, K. (2018b), "3D particlebased DEM investigation into the shear behaviour of incipient rock cracks with various geometries of rock bridges", *Rock Mech. Rock Eng.*, **51**, 3563-3584. https://doi.org/10.1007/s00603-018-1531-0

Shang, J., Duan, K., Gui, Y., Handley, K. and Zhao, Z. (2018c), "Numerical investigation of the direct tensile behaviour of laminated and transversely isotropic rocks containing incipient bedding planes with different strengths", *Comput. Geotech.*, **104**, 373-388. https://doi.org/10.1016/j.compgeo.2017.11.007

Tran, K.Q., Satomi, T. and Takahashi, H. (2019), "Tensile behaviors of natural fiber and cement reinforced soil subjected to direct tensile test", *J. Build. Eng.*, **24**, 100748. https://doi.org/10.1016/j.jobe.2019.100748

Vasarhelyi, B. and Bobet, A. (2000), "Modeling of crack initiation, propagation and coalescence in uniaxial compression", *Rock Mech. Rock. Eng.*, **33**(2), 119-139. https://doi.org/10.1007/s006030050038

Wang, Y., Zhou, X. and Xu, X. (2016), "Numerical simulation of propagation and coalescence of flaws in rock materials under compressive loads using the extended non-ordinary state-based peridynamics", *Eng. Fract. Mech.*, **163**, 273-248. https://doi.org/10.1016/j.engfracmech.2016.06.013

Wong, L.N.Y. and Einstein, H.H. (2009a), "Crack coalescence in molded gypsum and Carrara marble: part 1. Macroscopic observations and interpretation", *Rock Mech. Rock Eng.*, **42**(3), 475-511. https://doi.org/10.1007/s00603-008-0002-4

Wong, L.N.Y. and Einstein, H.H. (2009b), "Crack coalescence in molded gypsum and Carrara marble: Part 2. Microscopic observations and interpretation", *Rock Mech. Rock Eng.*, **42**(3), 513-545. https://doi.org/10.1007/s00603-008-0003-3

Yaylac, M, (2016), "The investigation crack problem through numerical analysis", *Struct. Eng. Mech., Int. J.*, **57**(6), 1143-1156. https://doi.org/10.12989/sem.2016.57.6.1143

Zhang, X.P. and Wong, L.N.Y. (2013), "Crack initiation, propagation and coalescence in rock-like material containing two flaws: a numerical study based on bonded-particle model approach", *Rock Mech. Rock Eng.*, **46**(5), 1001-1021. https://doi.org/10.1007/s00603-012-0323-1

Zhang, H., He, Y., Han, L., Jiang, B., Liang, Z. and Zhong, S. (2009), "Microfracturing characteristics in brittle material containing structural defects under biaxial loading", *Comput. Mater. Sci.*, **46**(3), 682-686. https://doi.org/10.1016/j.commatsci.2009.05.015

Zhang, J.Z., Zhou, X.P., Zhou, L.S. and Berto, F. (2019), "Progressive failure of brittle rocks with non-isometric flaws: Insights from acousto-optic-mechanical (AOM) data", *Fatigue Fract. Eng. Mater. Struct.*, **42**(8), 1787-1802. https://doi.org/10.1111/ffe.13019

Zhou, X.P., Bi, J. and Qian, Q.H. (2015), "Numerical simulation of crack growth and coalescence in rock-like materials containing multiple pre-existing flaws", *Rock Mech. Rock Eng.*, **48**, 1097-1114. https://doi.org/10.1007/s00603-014-0627-4

Zhou, X., Wang, Y. and Xu, X. (2016), "Numerical simulation of initiation, propagation and coalescence of cracks using the non-ordinary state-based peridynamics", *Int. J. Fract.*, **201**(2), 213-234. https://doi.org/10.1007/s10704-016-0126-6

Zhou, X.P., Zhang, J.Z., Qian, Q.H. and Niu, Y. (2019), "Experimental investigation of progressive cracking processes in granite under uniaxial loading using digital imaging and AE techniques", *J. Struct. Geol.*, **126**, 129-145. https://doi.org/10.1016/j.jsg.2019.06.003

Zhou, X.P., Zhang, J.Z. and Berto, F. (2020), "Fracture analysis in

brittle sandstone by digital imaging and AE techniques: Role of flaw length ratio", *J. Mater. Civil Eng.*, **32**(5), 04020085. https://doi.org/10.1061/(ASCE)MT.1943-5533.0003151

CC